FLUORESCENCE: POISSON STATISTICS AND ALGORITHMS FOR SPECTRAL DECOMPOSITION

ERVIN MUSTAFIĆ

Fakulteta za matematiko in fiziko
Univerza v Ljubljani

Fluorescence microscopy is a key technique in biophysics, yet its quantitative interpretation is often limited by spectral crosstalk and noise. In this paper, the photon counting statistics of fluorescence emission are examined, and it is experimentally confirmed that, under typical imaging conditions, detected photons follow Poisson statistics. Small deviations are observed only at high fluorophore concentrations, where fluorescence quenching becomes significant. This result is essential for spectral decomposition, as the Richardson–Lucy unmixing algorithm relies on a Poisson noise model. A comparison between the standard linear unmixing algorithm and the Richardson–Lucy algorithm is performed, showing that the latter provides superior performance, especially in the case of low signal-to-noise ratio data. Together, these findings demonstrate that improved multicolor fluorescence imaging and more reliable biological interpretation are enabled by accurate unmixing algorithms.

FLUORESCENCA: POISSONOVA STATISTIKA IN ALGORITMI ZA SPEKTRALNO DEKOMPOZICIJO

Fluorescenčna mikroskopija je ena izmed ključnih tehnik v biofiziki, vendar je njena kvantitativna analiza pogosto omejena zaradi prekrivanja emisijskih spektrov in šuma. V tem članku je proces štetja fotonov pri fluorescenci statistično analiziran, pri čemer je eksperimentalno pokazano, da pri tipičnih pogojih slikanja zaznani fotoni sledijo Poissonovi statistiki. Manjša odstopanja so opažena le pri visokih koncentracijah fluoroforja, kjer pride do potlačitve fluorescence. Ta rezultat je ključen za spektralno dekompozicijo rezultatov, saj se Richardson–Lucy algoritem opira na Poissonov model za opis fluorescence. V članku je izvedena primerjava med pogosto uporabljenim algoritmom linearne dekompozicije slik in Richardson–Lucy algoritmom, pri čemer je pokazano, da slednji zagotavlja boljše rezultate, zlasti pri meritvah z nizkim razmerjem signal–šum. Ti rezultati nakazujejo, da algoritmi, ki temeljijo na ustrezni statistiki fizikalnega pojava, omogočajo izboljšano večbarvno fluorescenčno mikroskopijo in s tem zanesljivejšo biološko interpretacijo.

1. Introduction

Fluorescence is one of the most powerful techniques in biophysics because it allows researchers to visualize and quantify specific molecules inside complex biological systems. It relies on fluorophores that absorb light and re-emit it at longer wavelengths, thereby converting molecular information into detectable photon signals. In microscopy, this makes it possible to track multiple structures and processes in parallel. However, using several fluorophores at once introduces a fundamental challenge: their emission spectra overlap. Detectors therefore record mixed signals in which photons from different dyes contribute to the same detection channel. This spectral crosstalk limits the accuracy of multicolor imaging and can obscure true biological differences. To recover clean per-fluorophore signals, modern workflows rely on spectral decomposition algorithms. Their performance is inherently linked to the statistics of fluorescence itself. Photon emission and detection are stochastic processes, and the number of detected photons follows Poisson statistics. These statistics define how photon counts fluctuate from frame to frame, and spectral decomposition must take this inherent variability into account when separating overlapping signals. Understanding this interplay between spectral overlap and Poisson-distributed photon counts is therefore essential for quantitative fluorescence microscopy. It motivates the development of robust decomposition methods that expand the number of usable fluorophores, minimize crosstalk, and ultimately yield cleaner, more reliable biological images.

2. Fluorescence

The emission of light that occurs from electronically excited states of a substance is called luminescence. This is further divided into fluorescence and phosphorescence, depending on the nature of the excited state. Fluorescence occurs when a molecule absorbs a photon and is promoted from its singlet state S_0 to an excited singlet state S_1 (or higher), after which it relaxes and emits a photon while returning to S_0. The relaxation process takes place on a nanosecond timescale. Looking at the Jablonski diagram in Fig. 1, singlet ground and first electronic states are depicted by S_0 and S_1, respectively. At each electronic energy level, the molecule possesses a set of vibrational sublevels $(0, 1, 2, 3, \dots)$. However, at room temperature, the available thermal energy is too small to populate the higher vibrational states appreciably, so levels such as 2 and 3 remain essentially unoccupied. The absorption and emission of light are shown as vertical lines to illustrate transitions between states. Absorption takes place on a femtosecond timescale, far too fast for the much heavier atomic nuclei to move. Consequently, the electronic transition occurs at essentially fixed nuclear positions — the essence of the Franck–Condon principle [1], [2]. Because these fixed positions rarely coincide with the vibrational minimum of the excited electronic state, the vertical transition typically lands on a vibrationally excited level of that state. Thus, after absorbing light, the molecule is promoted not only to a higher electronic state (e.g., S_1 or S_2) but also to a higher vibrational level, as illustrated in Fig. 1.

In most cases electrons then rapidly relax into the lowest vibrational state of S_1, a process also known as non-radiative or internal conversion which occurs in some picoseconds. The return to the ground state typically occurs to a higher excited vibrational ground state level. This is reflected in emission spectra often being a mirror or near-mirror image of absorption spectra as nuclear geometry is not greatly altered [1]. Jablonski diagrams also shows us that the energy of emission is typically less than of the absorption, a phenomenon known as Stokes shift [1], [2]. Fluorescent substances are called fluorophores (or fluorochromes), and they are typically aromatic molecules – ring-shaped structures with a fully delocalized π-electron system, which gives them stable, well-defined electronic energy levels.

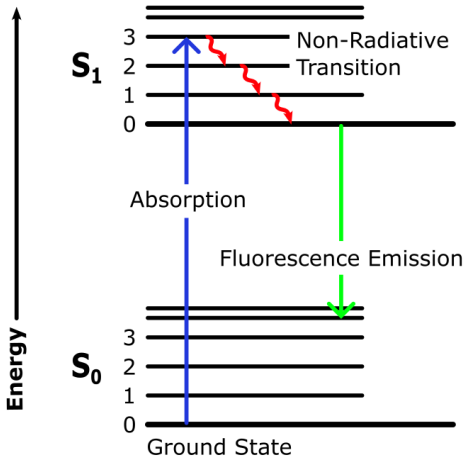

Figure 1. Jablonski diagram of fluorescence. In this case, an electron is excited by absorption into a higher vibrational level of the first excited electronic singlet state S_1. It then undergoes rapid non-radiative relaxation to the lowest vibrational level of S_1. Fluorescence emission occurs as the electron relaxes radiatively back to the ground electronic state S_0. Because part of the absorbed energy is dissipated non-radiatively, the emitted photon has lower energy (longer wavelength) than the absorbed photon.

3. Fluorescence Microscopy

Fluorescence microscopy is widely used because it enables researchers to visualize specific molecules with high sensitivity and selectivity, often even in living cells. By labeling different components with fluorophores, it becomes possible to monitor structure, dynamics, and interactions that are otherwise invisible under conventional microscopy. Because the fluorescence process occurs on very short timescales, its detection requires sophisticated electronics and optics [1]. A widely used approach to fluorescence detection is epifluorescence microscopy, in which excitation and emission light share the same objective lens, as depicted in the left part of Fig. 2. This geometry maximizes both illumination of the fluorophores and collection of the emitted photons, which is crucial because fluorescence signals are typically orders of magnitude

weaker than the excitation light. With the appropriate optical filters, the strong excitation beam can then be rejected, allowing only the desired fluorescence to reach the detector and produce high-contrast images. Using the same objective for excitation and detection ensures that the illuminated area of the sample is exactly the area being imaged, which is essential for efficient fluorescence collection [1], [2].

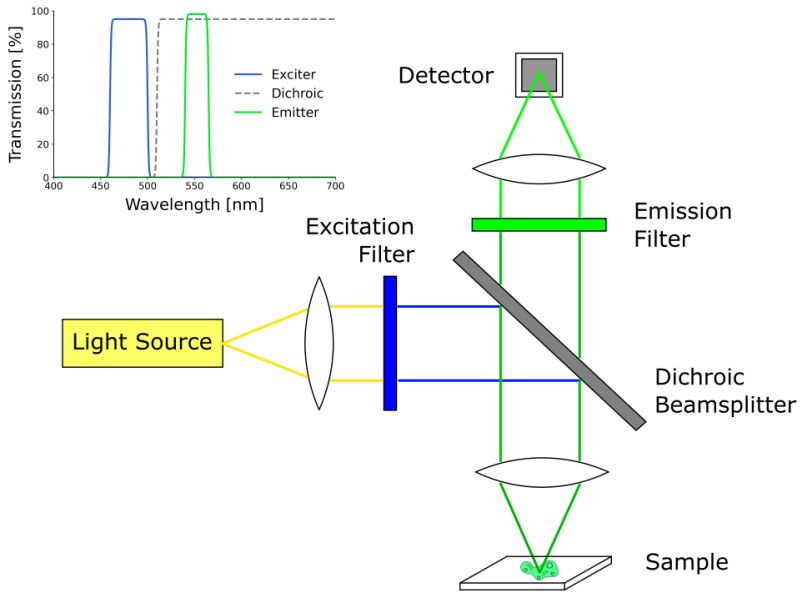

Figure 2. Configuration used in epifluorescence microscopy with an example of transmission graphs for filters that are used when imaging fluorophores.

We rely on optical filters rather than monochromators for wavelength selection. Looking at Fig. 2, we also have a dichroic beamsplitter which reflects the excitation wavelengths into the objective, transmits the emission from fluorophores and allows it to reach the eyepiece or detector. The function of these optical filters is to let only the specific wavelengths pass through. The emission filter transmits the emission and rejects the excitation wavelengths, and vice versa for the excitation filter. Because of the Stokes shift, the emission filter for a given fluorophore is chosen to transmit wavelengths that are longer than the wavelengths selected by its excitation filter. However, this relationship holds only within a fluorophore–filter pair, not necessarily across different dyes or filter sets. Transmission graphs for our filters can be seen on the upper left part of Fig. 2 [1].

Fluorescence microscopy is often performed with multiple fluorophores to label different cell organelles [3]. Now, emission filters have been designed to pass the emission from many fluorophores – we call them multi-bandpass filters [1]. One important limitation of fluorescence microscopy is photobleaching: each fluorophore can emit only a finite number of photons before becoming permanently nonfluorescent [3]. Photobleaching, together with detector sensitivity and background fluorescence, constrains the amount of usable signal that can be collected from a sample. When multiple fluorophores are used simultaneously, an additional and far more fundamental challenge emerges: their emission spectra overlap. This causes detectors to record mixtures of signals from different fluorophores, severely complicating quantitative analysis [1], [2]. The use of specific fluorescence filtersets (dichroic beamsplitter, excitation filter and emission filter) achieves a reliable separation of the signals of the most used fluorophore combinations, but it does not solve the problem entirely [4].

4. Fluorophore Crosstalk

In multicolor fluorescence microscopy, the goal is to measure the contribution of each fluorophore independently, even though they are imaged simultaneously. Ideally, each detection channel would record photons originating from only one fluorophore, making it straightforward to assign signals to specific molecular species. In practice, however, this separation is rarely perfect. Emission of the fluorophore MTG across multiple channels is shown in Fig. 3.

Fluorophore crosstalk (also called bleed-through or leakage) arises because emission spectra of different fluorophores partially overlap [4]. When this happens, a detector that is nominally assigned to one fluorophore will also record photons emitted by others. A related effect is cross-excitation: excitation light intended for one fluorophore may also excite another with appreciable efficiency [4]. As modern experiments often use multiple fluorophores simultaneously, these forms of crosstalk generalize to mixtures involving many fluorophores, and separating their contributions becomes a central analytical challenge.

We can see that fluorophore crosstalk is essentially a fundamental problem that arises from the nature of fluorophores' wide emission and absorption spectra [1]. We can try to solve this problem by using fluorophores whose emission spectra are as far away as possible. But even then, some of the spectra still overlap. Separation of signal is only possible because of the spectra characteristics:

1. Excitation spectra has long tails to the shorter wavelength and rapid drop after the excitation maximum.

2. Emission spectra has rapid rise to the emission maximum and a long tail to the longer wavelengths.

But this only works for two fluorophores under the assumption that we have a matching filtersets designed just for these two fluorophores. If we look at the currently available fluorescent proteins, we can see that their wide spectral distribution is not often matched to existing filtersets and due to their brightness sensitivity and pH stability, just to name a few, they cannot readily be "mixed and matched" solely on their spectral properties. Viable combinations present a significant problem with crosstalk [4]. Additional complications arise from the need to use sequential acquisition of the different channels if we are using specific filtersets for multichannel imaging, as this prolongs our data gathering process. In this time, a living sample may change, or the observed process may happen faster than we can gather the signal from all channels [4].

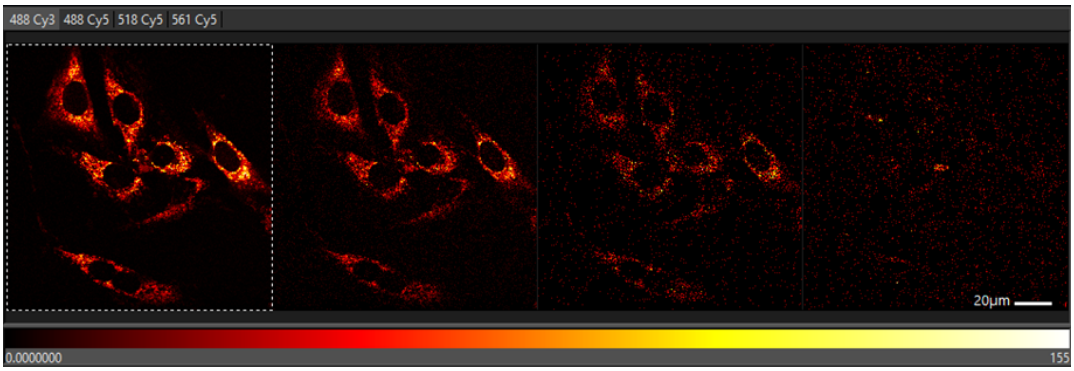

Figure 3. Example of fluorophore emission detection. The same sample with fluorophore MTG is imaged in four different detection channels. Each channel represents a specific optical pathway defined by a chosen excitation wavelength and a corresponding set of emission filters and detectors. Colorbar is in photon counts. Image was taken at Jožef Stefan Institute, Department of Condensed Matter Physics, Laboratory for Biophysics, Ljubljana.

Some fluorophores are significantly brighter than the others. Combinations of dim and bright fluorophores can cause problems when identifying the signals of the dim fluorophores. Same happens if both fluorophores are equally bright, but the concentration of one is larger than the other [4].

5. Poisson Statistics of Fluorescence Emission

In fluorescence microscopy we detect individual photons produced by stochastic excitation–emission events in many fluorophores. Each fluorophore can absorb a photon, relax, and emit again, but the

exact timing of each emission is random. When many independent fluorophores are illuminated continuously, these emission events occur at a constant average rate, and the number of detected photons in each time interval follows Poisson statistics. This is a general consequence of having many independent emitters producing rare, uncorrelated events. Although single-molecule experiments reveal quantum features such as antibunching [5], these effects vanish when observing large ensembles. In conventional imaging the detector integrates light from thousands of molecules, and the resulting photon counts behave as a Poisson process. This statistical model is fundamental for quantitative microscopy, because it determines the uncertainty in each pixel and therefore limits how accurately overlapping spectral signals can be unmixed.

5.1 Experiment to Show that Fluorescence Emission Really Is Poisson-distributed

To experimentally verify that fluorescence emission follows Poisson statistics, we measured the distribution of detected photons under controlled conditions at Jožef Stefan Institute, Department of Condensed Matter Physics, Laboratory for Biophysics. Fluorescence emission depends on the local fluorophore concentration, the excitation intensity, the absorption cross-section, and the quantum yield [7]. These parameters determine how many photons are produced in each pixel and therefore set the expected mean photon count used in spectral decomposition (also called unmixing).

Experimental setup consists of the following excitation lasers: 488 nm at 75 μW power, 561 nm at 70 μW power and 640 nm at 235 μW power. Emission was measured on Abberior microscope setup, equipped with a single-point photon-counting detector with pixel size 200 nm. We used three filters: 500–548 nm, 581–627 nm and 651–720 nm. We selected four fluorophores whose excitation and emission bands span a broad portion of the visible spectrum:

- Fluorescein (λ_{abs}=460 nm, λ_{em}=515 nm),
- Star 580 NHS (λ_{abs}=587 nm, λ_{em}=607 nm),
- Atto 594 NHS (λ_{abs}=601 nm, λ_{em}=634 nm),
- Alexa Fluor 647 (λ_{abs}=651 nm, λ_{em}=672 nm).

For each fluorophore we prepared solutions at 0.1 μM, 1.0 μM and 10.0 μM concentrations (except in the case of Alexa Fluor 647 due to limited supply). For each solution, ten measurements were made under the same conditions. With this approach we could estimate the photon-count statistics for each fluorophore-concentration pair and see how much it deviated from ideal Poisson.

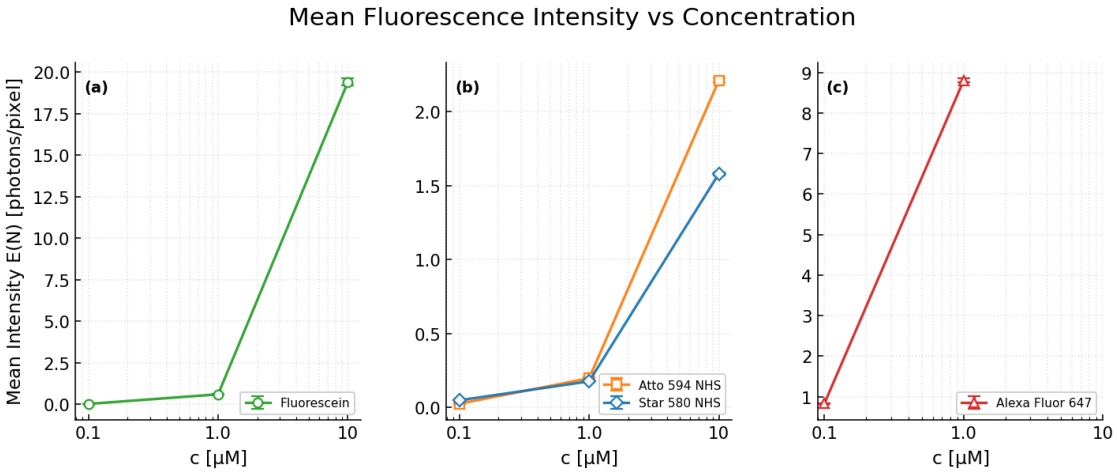

Figure 4. Mean fluorescence intensity at different concentrations for all fluorophores are shown in **a)**, **b)** and **c)**. We can see that the range of mean intensity E(N) changes for different fluorophores, but they all follow a similar trend. We are missing 10.0 μM of Alexa Fluor 647 due to limited supply.

We defined Fano factor as [6]

$$k = \frac{\mathrm{Var}(N)}{\mathrm{E}(N)}$$

where $\mathrm{Var}(N)$ is variance of detected photons N and $\mathrm{E}(N)$ is the mean number of detected photons N. In ideal Poisson distributions, our Fano factor is $k = 1$. We fit a linear function $y = kx$ with no offset. Raw data is shown in Fig. 4, where in **a)** we can see fluorescein, in **b)** Atto 594 NHS and Star 580 NHS and in **c)** Alexa Fluor 647.

Combined results of all fluorophores, grouped by concentration, are shown in histogram **A** in Fig. 5. We can see that in the case of all concentrations Fano factors lie within error range of the ideal Poisson value. However, in the case of 10.0 μM we can see a small deviation from ideal Poisson (but it is still in the error range of ideal Poisson), likely due to quenching of fluorescence. When an excited fluorophore molecule collides with another molecule before emitting, it returns to the ground state non-radiatively [1], [2]. Combining the Fano factors of all the concentrations we obtain

$$k = (1.006 \pm 0.003)\ \text{photons/pixel}.$$

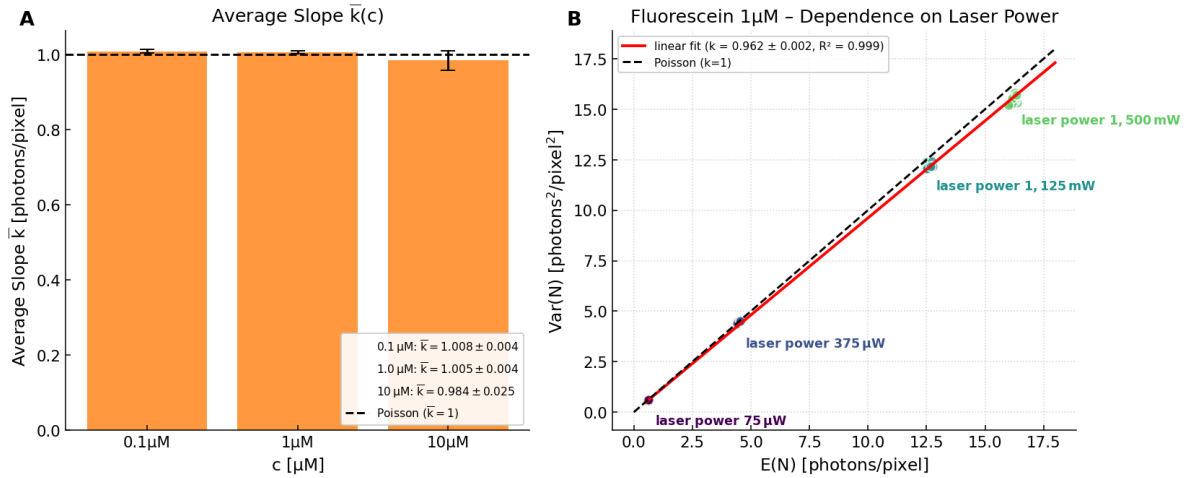

Figure 5. **A**: average Fano factors of fluorophores, grouped into three different concentrations. We can see that we are in the range of ideal Poisson. **B**: in the case of fluorescein 1.0 μM, we see that Poisson distribution is almost independent of laser power.

Another thing we analyzed was how different laser powers of excitation laser 488 nm affect fluorescence emission. Panel **B** of Fig. 5 shows that for four different laser powers 75 μW, 375 μW, 1, 125 mW and 1, 500 mW we observe only a slight deviation from Poisson distribution, which implies that Poisson distribution is almost independent of laser power. Linear regression yielded $k = (0.962 \pm 0.002)$ photons/pixel which is marginally in the sub-Poisson region. This small deviation may be attributed to the onset of fluorophore saturation – under strong excitation, fluorophores enter saturation, spending a finite time in the excited state during which they cannot emit again. This suppresses short-timescale fluctuations and yields variance slightly below the Poisson expectation.

6. Algorithms for Spectral Decomposition

The experiment described in Section 5.1 shows that photon detection in fluorescence microscopy follows Poisson statistics. The statistical properties of the detected signal strongly influence which

spectral decomposition algorithms are appropriate. In particular, algorithms that explicitly account for Poisson noise, such as the Richardson–Lucy algorithm, can exploit this property to improve the estimation of fluorophore contributions.

As discussed in Sections 3. and 4. , standard fluorescence imaging approaches cannot meet some of the current experimental requirements of biological imaging [4]. To address the problem of spectral crosstalk, several image analysis approaches have been proposed, including supervised classification analysis, principal component analysis, linear unmixing, Richardson–Lucy unmixing, and Bayesian unmixing. The first two are classification-based – they try to classify each pixel into one fluorophore category based on its spectral signature. These techniques, however, do not work for colocalized fluorophore signals such as those found in tissues or cells but have worked in spectral karyotyping using multicolor FisH [4]. It has been shown that linear unmixing, Richardson–Lucy unmixing and Bayesian unmixing are the best suited to analyze mixed contributions to a pixel, as would be the case for colocalizing labels [4], [7], [8], [9].

Spectral decomposition allows us to effectively separate fluorescent signals from combined images and helps us with better visualization and interpretation of biological samples [7].

6.1 Linear Unmixing

To quantify spectral crosstalk, we define leakage coefficients a_{ij} that describe how strongly fluorophore j contributes to detector i. It depends on the excitation intensity I, the fluorophore's quantum yield η, and its molar absorption coefficient ϵ. Higher fluorescence emission or stronger spectral overlap increase the leakage term. Let $[A]$ be the matrix of leakage coefficients a_{ij}, $[I_{\text{det}}]$ the vector of measured detector intensities and $[S]$ the vector of photons emitted by each fluorophore into its optimal detection channel [7]. The measured signal follows a linear mixing model

$$[I_{\text{det}}] = [A][S] \tag{1}$$

where columns of $[A]$ correspond to fluorophores and rows of $[A]$ correspond to detectors. All leakage coefficients are non-negative because every fluorophore contributes additively to the detected signal. To recover the true fluorophore contributions, we must take

$$[S] = [A]^{-1}[I_{\text{det}}].$$

For complete derivation of linear unmixing, the reader is referred to [7]. If $[A]$ is square, meaning that we have the same number of detectors and fluorophores, we compute a standard inverse. If not, we use the Moore-Penrose pseudoinverse. A minimal pseudocode implementation is shown in Fig. 1. Mathematically speaking, linear unmixing corresponds to solving an inverse problem given the measured detector intensities and the mixing matrix, recovering the underlying fluorophore signals.

Algorithm 1: Implementation of a linear spectral unmixing.

Data: $[A]$ (mixing matrix), $[I_{\text{det}}]$ (detector intensities)
Result: $[S]$ (estimate of unmixed spectra)
Compute $[A]^{-1}$; `// inverse or pseudoinverse`
$[S] \leftarrow [A]^{-1}\,[I_{\text{det}}]$;
return $[S]$;

6.2 Richardson–Lucy Unmixing

A practical limitation of linear unmixing is that it does not account for Poisson noise, which dominates fluorescence imaging. When the signal is low or noise is high, the matrix inversion in linear

unmixing can easily produce negative photon counts, which are physically meaningless. This is a direct consequence of treating the problem as a purely algebraic inversion, without modelling the underlying statistics of photon emission.

To address this, we use the Richardson–Lucy unmixing (abbreviated RLSU), an algorithm that explicitly models Poisson-distributed photon counts which is the case when dealing with the detection of fluorescence as shown in Section 5.1 . Since the detection of fluorescence follows Poisson statistics, incorporating this noise model leads to a much more robust and physically consistent estimate of fluorophore contributions, especially at low signal levels [8]. Originally, the Richardson–Lucy algorithm was developed for image deconvolution using a known point spread function PSF. However, the method applies to any system that can be described by a linear forward operator with Poisson noise [8]. In our case, the forward operator is not a convolution but the mixing matrix $[A]$, the same matrix used in linear unmixing with the distinction that the sum of each column is 1.0 which forces the conservation of the photon number. Because the true fluorophore contributions $[S]$ cannot be recovered by a single matrix inversion, they must be estimated iteratively, gradually improving the estimate so that the predicted detector signal $[I_{\text{det}}] = [A][S]$ becomes consistent with the measured noisy data $[d]$. This leads to an iterative refinement procedure as shown in Fig. 2:

- start with an initial positive guess S_0,
- compare the measured data d with the predicted detector signal, calculated using Eq. 1,
- update the estimate so that the next iteration better explains the measured counts under a Poisson noise model.

By starting from a non-negative initial estimate $[S_0]$, the algorithm can never produce negative photon counts, because every update consists only of element-wise multiplications with non-negative factors. The update equation is

$$[S_{t+1}] = [S_t] \cdot [A]^\top \left(\frac{[d]}{[A][S_t]} \right).$$

Algorithm 2: Implementation of the Richardson–Lucy spectral unmixing.

Data: $[d]$ (measured data), $[A]$ (mixing matrix), T (no. of iterations)
Result: $[S]$ (estimate of unmixed spectra)
$[S] \leftarrow [S_0]$; `// [S_0] can be a matrix of ones`
$t \leftarrow 0$;
while $t < T$ **do**
  $r \leftarrow [d]/([A]\,[S])$;
  $S \leftarrow [S] \cdot [A]^\top r$;
  $t \leftarrow t + 1$;
return $[S]$;

It has been shown that if we also use PSF alongside the mixing matrix $[A]$ so that we also perform deconvolution, the Richardson–Lucy algorithm tends to prefer sparse solutions and can overfit noise, which manifests as high-frequency artifacts in the reconstruction. This is due to divergence of PSF linear operator with iterations, whereas unmixing solely converges. The appearance and structure of these artifacts depend strongly on the number of iterations T, which are typically hand-tuned to obtain a visually acceptable result. Because RLSU maximizes a Poisson likelihood without explicit regularization, noise amplification and poor convergence behavior are intrinsic to the method if we

also use PSF. Interestingly, during the iterative process the algorithm first reconstructs genuine high-frequency signal components, while the amplification of noise emerges only at later iterations. Thus, RLSU often produces good early-iteration estimates, but prolonged iteration leads to artifact growth [9], [10].

6.3 Mathematical Formalism of Spectral Decomposition

We introduce two mathematical spaces. The first is the *detector space*, which contains the measured detector signals, so raw photon counts that are subject to Poisson noise. The second is the *fluorophore space*, whose components correspond to the individual fluorophores present in the sample. The dimension of the detector space is the number of detectors, whereas the dimension of the fluorophore space is the number of fluorophores. Figurative representation is shown in Fig. 6. The objective of spectral decomposition algorithms is to map the measured photon counts from detector space onto fluorophore space via a crosstalk matrix $[A]$.

This perspective provides a key insight: the primary quantity of interest is not the signal observed by the detector itself, but rather the spatial and quantitative distribution of fluorophores bound within the sample. The detector signal is merely an intermediate representation. If we assume the absence of spectral crosstalk, the mixing matrix $[A]$ reduces to the identity matrix after appropriate ordering of the rows of $[A]$. In this special case, detector space and fluorophore space coincide, and each detector channel directly corresponds to a single fluorophore without mutual spectral overlap.

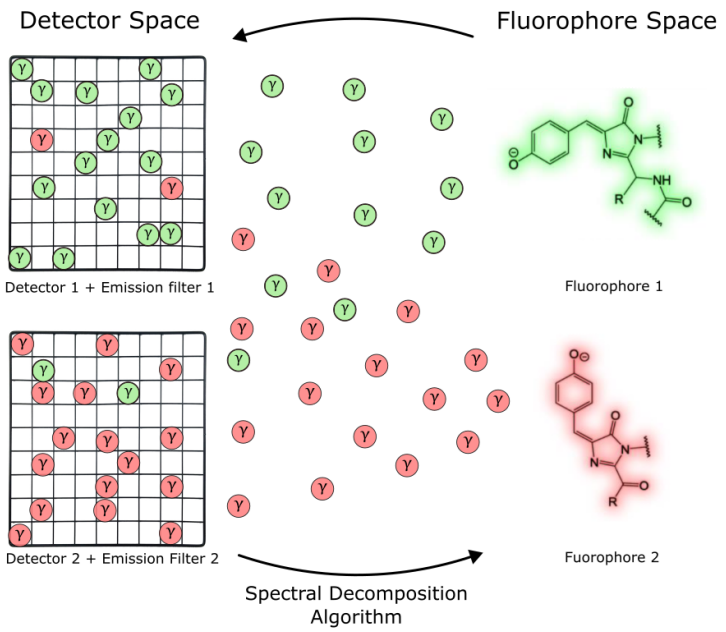

Figure 6. Figurative representation of detector and fluorophore space. Emitted photons originate from fluorophores and are captured by detectors. Each detector captures most photons from its designated fluorophore (e.g. detector 1 captures most photons from fluorophore 1), while also registering contributions from other fluorophores. Spectral decomposition algorithms are used to map signals between the two spaces. Adapted from [11], licensed under CC BY 4.0.

This formulation also provides a foundation for a group-theoretical description of the problem. Although the quantities of interest reside in fluorophore space, the raw photon counts in detector space play a fundamental role, as they represent invariants of the spectral decomposition. Preserving these detector-space measurements is therefore essential when storing experimental data, since they contain the information required to reconstruct fluorophore contributions under different decomposition models.

6.4 Comparison of Linear and Richardson–Lucy Unmixing

The main disadvantage of linear unmixing is its poor decomposition compared to Richardson–Lucy unmixing, with more errors associated with unmixing lower signal-to-noise ratio data. Linear unmixing predicted negative photon number in many pixels, which is nonphysical. This occurs because linear unmixing is incapable of dealing with Poisson noise which is the dominant noise source in low

signal-to-noise ratio images, as shown in Section 6.2 [8]. According to the literature [8], Richardson–Lucy unmixing shows that although one iteration is insufficient to accurately unmix the different components, 100 iterations produce a higher quality result than linear unmixing, even when negative values in linear unmixing are set to zero. Notably, no negative values are generated with Richardson–Lucy unmixing as the initial estimate is positive in every element, and the iterative update is multiplicative. Repeating this process for different signal-to-noise ratios while incorporating both Poisson noise and read noise from detectors, Richardson–Lucy always outperformed linear unmixing [8]. Richardson–Lucy unmixing outperforms linear unmixing when dealing with highly overlapping spectra (20 nm peak-to-peak separation) and can unmix signals with a peak-to-peak spectral separation as low as 4 nm using only two detectors [8].

Panel **A** in Fig. 7 illustrates a simulated benchmark dataset consisting of eight objects (letters), each assigned a distinct fluorophore. The authors generate synthetic measurements by applying the mixing matrix and adding Poisson noise, mimicking real detector statistics. They then attempt to recover the underlying spectra using linear unmixing as well as Richardson–Lucy unmixing with 1 and 100 iterations. Linear unmixing fails to reconstruct the letters cleanly, whereas RLSU progressively improves the reconstruction and approaches the ground truth with increasing iteration count. Panel **B** in Fig. 7 shows results on an experimentally acquired dataset of a U2OS cell coexpressing six fluorescent proteins. Linear unmixing produces negative values (displayed in red) and misassigns signals; for example, Golgi fluorescence appears incorrectly in the mitochondria channel. Panel **C** in Fig. 7 presents the corresponding RLSU result, which exhibits accurate spectral separation with no observable bleed-through between channels [8].

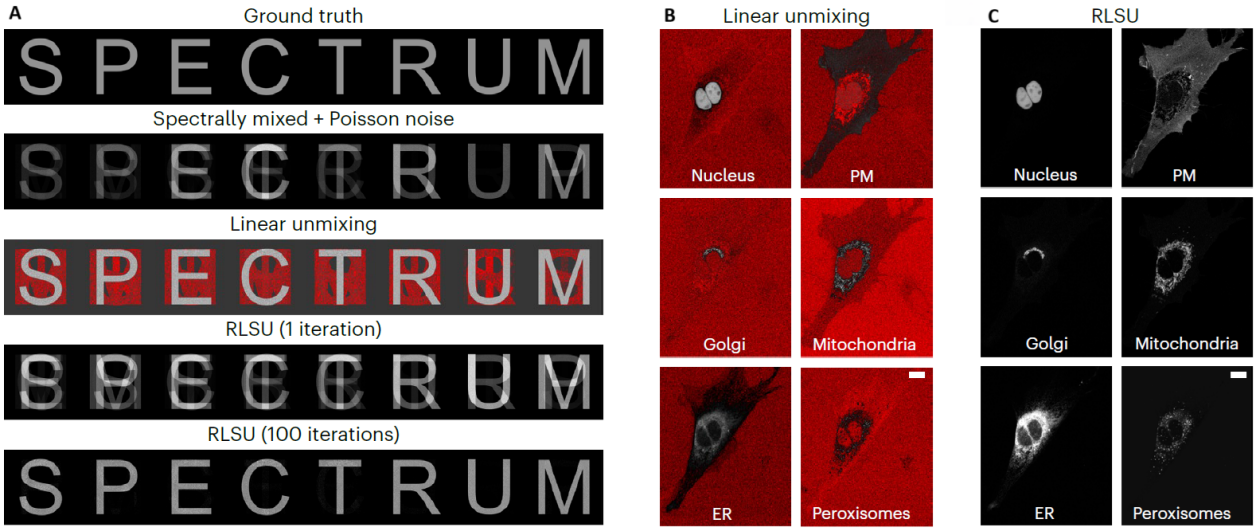

Figure 7. Comparison of linear unmixing and Richardson–Lucy spectral unmixing on simulated and experimental datasets (adapted from the results presented in [8], licensed under CC BY 4.0). Panel **A** shows a simulated benchmark in which eight objects (the letters of "SPECTRUM") are assigned eight different fluorophores. After spectral mixing and addition of Poisson noise, linear unmixing produces strong artefacts and negative values, shown in red, whereas RLSU progressively reconstructs the ground truth, achieving near-perfect recovery after 100 iterations. Panels **B** and **C** show an experimentally acquired U2OS cell expressing six fluorescent proteins. Linear unmixing misassigns signals between channels (e.g., Golgi signal leaking into the mitochondria channel) and produces negative intensities. In contrast, RLSU yields clean spectral separation with no observable bleed-through. Scale bars: 10 μm.

7. Conclusions

In this paper we experimentally verified that the detection of fluorescence follows Poisson statistics, with small deviations appearing only at very high fluorophore concentrations of 10.0 μM. This confirms that Poisson-based noise models provide an appropriate statistical description of fluorescence

microscopy data. This result is directly relevant for spectral decomposition algorithms. In particular, the Richardson–Lucy spectral unmixing (RLSU) algorithm is explicitly derived under the assumption of Poisson photon statistics. Our results therefore provide experimental support for the assumptions underlying this method. In practice, this means that RLSU can make better use of the statistical properties of photon detection when estimating fluorophore contributions from detector measurements.

We further showed that the Richardson–Lucy algorithm provides a more reliable separation of overlapping fluorophore emission signals than standard linear unmixing. This is especially important in modern biological imaging, where multiple fluorophores with partially overlapping emission spectra are often used simultaneously. Improved spectral decomposition allows researchers to interpret fluorescence signals more accurately and to distinguish between different labeled structures inside biological samples. Beyond fluorescence microscopy, the ideas discussed in this work may also have broader relevance for other imaging and signal-processing problems where measurements consist of discrete photon counts or other Poisson-distributed signals. In such cases, algorithms that explicitly incorporate the correct statistical model of the data can provide more accurate reconstructions and improved interpretation of experimental measurements.

Together, these results highlight the importance of understanding photon statistics and using appropriate statistical models in image reconstruction algorithms. Combining experimental insight with suitable computational methods can significantly improve the reliability of fluorescence imaging and support more precise quantitative analysis in biological research.

REFERENCES

[1] J.R. Lakowicz, *Principles of Fluorescence Microscopy*, Third Edition, Springer, 2006.

[2] J.W. Lichtman, J.-A. Conchello, *Fluorescence Microscopy*, Nature Methods **2** (2005), no. 12, 910–919.

[3] J.B. Pawley, *Handbook of Biological Confocal Microscopy*, Third Edition, Springer, 2006.

[4] T. Zimmermann, J. Marrison, K. Hogg, P. O'Toole, *Clearing Up the Signal: Spectral Imaging and Linear Unmixing in Fluorescence Microscopy*, Methods in Molecular Biology **1075** (2014), 129–148.

[5] H.F. Arnoldus, G. Nienhuis, *Photon Statistics of Fluorescence Radiation*, Optica Acta **33** (1986), no. 6, 691–702.

[6] K. Rajdl, P. Lánský, *Fano Factor Estimation*, Mathematical Biosciences and Engineering **11** (2014), no. 1, 105–123.

[7] A. Bajrić, *Three-colour STED Microscopy*, Master's thesis, University of Ljubljana, Slovenia, 2025.

[8] A. Kumar, K. E. McNally, Y. Zhang, A. Haslett-Saunders, X. Wang, J. Guillem-Marti, D. Lee, B. Huang, S. Stallinga, R. R. Kay, D. Baker, E. Derivery, and J. D. Manton, *Multispectral Live-Cell Imaging with Uncompromised Spatiotemporal Resolution*, Nature Photonics **19** (2025), 1146–1156.

[9] Z. H. Hendrix, P. T. Brown, T. Flanagan, D. P. Shepherd, A. Saurabh, and S. Pressé, *Re-thinking Richardson–Lucy without Iteration Cutoffs: Physically Motivated Bayesian Deconvolution*, arXiv preprint (2024), arXiv:2411.00991.

[10] Y. Liu, S. Panezai, Y. Wang, S. Stallinga, *Noise Amplification and Ill-Convergence of Richardson–Lucy Deconvolution*, Nature Communications **16** (2025), 911.

[11] C. Chen, J. N. Henderson, D. A. Ruchkin, J. M. Kirsh, M. S. Baranov, A. M. Bogdanov, J. H. Mills, S. G. Boxer, and C. Fang, *Structural Characterization of Fluorescent Proteins Using Tunable Femtosecond Stimulated Raman Spectroscopy*, Int. J. Mol. Sci. **24**(15) (2023), 11991.